1   Towards chemical validation of *Leishmania infantum*

2   ribose 5-phosphate isomerase as a drug target

3   **Emily A. Dickie**[a], **Céline Ronin**[b], Mónica Sá[c,d], Fabrice Ciesielski[b], Nathalie

4   Trouche[b], Joana Tavares[c,d], Nuno Santarem[c,d], Louise L. Major[a], Iain K. Pemberton[e],

5   Jane MacDougall[e], Terry K. Smith[a#], Anabela Cordeiro-da-Silva[c,d,f#] & Paola

6   Ciapetti[b#]

7   [a]Biomedical Sciences Research Complex, University of St. Andrews, St Andrews,

8   Fife, Scotland, UK;

9   [b]NovAliX, Biology Department, Illkirch Cedex, France

10   [c]i3S–Instituto de Investigação e Inovação em Saúde, Universidade do Porto, Porto,

11   Portugal;

12   [d]IBMC-Instituto de Biologia Molecular e Celular, Parasite Disease Group, Porto,

13   Portugal;

14   [e]Photeomix Protein Discovery, IP Research Consulting, Noisy Le Grand, France;

15   [f]Departmento de Ciências Biológicas, Faculdade de Farmácia, Universidade do

16   Porto, Porto, Portugal.

17

18   [#]Joint corresponding authors: Terry K. Smith, tks1@st-andrews.ac.uk

19   Paola Ciapetti, pciapetti@novalix.com

20   Anabela Cordeiro da Silva, cordeiro@ibmc.up.pt

21

22   Running title: *L. infantum* RpiB screening and structure

23   Keywords: Neglected tropical diseases, *Leishmania infantum*, leishmaniasis, ribose

24   5-phosphate isomerase, inhibitor, screening, thermal shift, anti-parasitic, protein

25   crystal structure

26

27   **Abstract**

28

29   Neglected tropical diseases caused by kinetoplastid parasites (*Trypanosoma brucei*,

30   *Trypanosoma cruzi* and *Leishmania* spp.) place a significant health and economic

31   burden on developing nations worldwide. Current therapies are largely out-dated,

32   inadequate and facing mounting drug resistance from the causative parasites. Thus,

33   there is an urgent need for drug discovery and development. Target-led drug

34   discovery approaches have focused on the identification of parasite enzymes

35   catalysing essential biochemical processes, which significantly differ from equivalent

36   proteins found in humans, thereby providing potentially exploitable therapeutic

37   windows. One such target is ribose 5-phosphate isomerase B (RpiB), an enzyme

38   involved in the non-oxidative branch of the pentose phosphate pathway, which

39   catalyses the inter-conversion of D-ribose 5-phosphate and D-ribulose 5-phosphate.

40   Although protozoan RpiB has been the focus of numerous targeted studies,

41   compounds capable of selectively inhibiting this parasite enzyme have not been

42   identified. Here, we present the results of a fragment library screening against

43   *Leishmania infantum* RpiB, performed using thermal shift analysis. Hit fragments

44   were shown to be effective inhibitors of *Li*RpiB in activity assays, and several were

45   capable of selectively inhibiting parasite growth *in vitro*. These results support the

46   identification of *Li*RpiB as a validated therapeutic target. The X-ray crystal structure

47   of apo *Li*RpiB was also solved, permitting docking studies to assess how hit

48   fragments might interact with *Li*RpiB to inhibit its activity. Overall, this work will guide

49   structure-based development of *Li*RpiB inhibitors as anti-leishmanial agents.

50

51

Introduction

The kinetoplastid protozoan parasites *Trypanosoma brucei*, *Trypanosoma cruzi* and *Leishmania* spp. are causative agents of the neglected tropical diseases (NTDs) human African trypanosomiasis (HAT), Chagas disease and leishmaniasis respectively. These NTDs continue to have a hugely damaging impact on global health and economies, yet currently available chemotherapeutic options are widely inadequate, and no effective human vaccines are available. Although significant progress has been made in recent years (1), particularly in the treatment of HAT (2), it has remained challenging to develop new drugs for leishmaniasis. Cutaneous leishmaniasis (CL) and visceral leishmaniasis (VL) pose a major health threat to an estimated 1 billion people, with over 1 million cases occurring annually, VL causing 20,000-30,000 deaths (3, 4). Although a number of therapeutic candidates are progressing into clinical trials (5), most are at early stages and further leads are required to off-set the often high attrition rates of clinical development. This is particularly true in the case of leishmaniasis where treatment complexity is heightened by the requirements of different regions, which experience infections driven by different leishmanial species that also exhibit differing drug susceptibilities. Thus, sustained efforts to identify new avenues for anti-leishmanial lead discovery are vital. This need has led to extensive research into the metabolism of *Leishmania* spp. parasites, with a view to establishing areas of biochemical divergence from their hosts that can be exploited to combat them whilst minimising potential side-effects.

The enzyme ribose-5-phosphate isomerase (Rpi) catalyses the isomerization of ribose-5-phosphate (R5P) to ribulose-5-phosphate (Ru5P) (Figure S1) in the non-

4

77 oxidative branch of the pentose phosphate pathway (PPP) (Figure 1) (6, 7).

78 Alongside glycolysis and the Kreb's cycle, the PPP was one of the first identified

79 metabolic pathways and is highly conserved in both prokaryotes and eukaryotes (8).

80 The PPP supports key cellular functions, with the non-oxidative branch providing

81 precursors for nucleotide, amino acid and vitamin biosynthesis, and the oxidative

82 branch contributing to redox regulation (8). Though the oxidative branch of the

83 pathway is confined to eukaryotes, the non-oxidative pathway is common to all

84 organisms. Two physically and genetically distinct forms of Rpi are known to exist

85 and were first characterised in *Escherichia coli* K12 (9), which produces both types.

86 RpiA is present in all taxonomic groups but RpiB has only been found in bacteria and

87 lower eukaryotes, including protozoa (10).

88 The fact RpiBs are found exclusively in lower eukaryotes, including human

89 pathogenic species, has led to them becoming the focus of numerous studies aiming

90 to establish their essentiality, solving their protein structure and identifying specific

91 inhibitors. Crystal structures for the RpiBs from *E. coli* and *Mycobacterium*

92 *tuberculosis* have been determined to facilitate targeted drug design (11–13).

93 Inhibition studies have centred on mimicking the structure of the high energy *cis-*

94 enediolate isomerisation reaction intermediate, such that inhibitors including 4-

95 phospho-D-erythronohydroxamic acid (4-PEH) have been identified (14). However,

96 these inhibitors lack selectivity for RpiBs, given RpiAs also catalyse isomerisation via

97 this high-energy intermediate, meaning they are unlikely to provide routes to the

98 development of novel, selective therapeutics.

99 The RpiBs from kinetoplastid parasites have also been examined. RpiB

100 downregulation through RNA interference (RNAi) in *T. brucei* decreased parasite *in*

5

101   *vitro* growth and the infectivity of bloodstream forms towards mice (15). Mice infected

102   with induced RNAi clones exhibited lower parasitaemia and a prolonged survival

103   compared to control mice. Phenotypic reversion was achieved by complementing

104   induced RNAi clones with an ectopic copy of the *Trypanosoma cruzi* gene (15). A

105   crystal structure for *T. cruzi* RpiB (*Tc*RpiB) has been determined (16), and research

106   into the enzyme's substrate specificity and potential inhibition has been conducted

107   (17). *Leishmania spp.* RpiB has been studied in *Leishmania donovani*, *Leishmania*

108   *major* and *Leishmania infantum* (10, 18, 19). In *L. infantum* null mutant generation

109   was only possible when an episomal copy of the RpiB gene was provided, and the

110   latter was preserved both *in vitro* and *in vivo* in the absence of drug pressure. This

111   indicates the gene is essential for parasite survival (19). Although kinetoplastid

112   RpiBs have also been shown to be susceptible to 4-PEH inhibition, no other specific

113   inhibitors have yet been identified, potentially as studies of these enzymes have

114   been largely dominated by structural modelling and *in silico* inhibition prediction (10,

115   20).

116   Here, we present the findings from a thermal shift (differential scanning fluorimetry)

117   fragment library screening against recombinantly expressed *L. infantum* RpiB

118   (*Li*RpiB). Hits obtained were analysed for their ability to inhibit *Li*RpiB via *in vitro*

119   activity assay and for their anti-parasitic potency in cell viability assays. Results

120   indicate that ability to interact with and effectively inhibit *Li*RpiB can be linked to anti-

121   parasitic efficacy, strengthening the case for *Li*RpiB as a validated drug target. We

122   have also determined the first X-ray crystal structure for a *Leishmania* spp. RpiB,

123   which permitted *in silico* docking analysis to speculate how the hit inhibitory

124   fragments identified during this research might bind and inhibit *Li*RpiB activity.

125 Overall, this work provides novel insight that will inform the design of kinetoplastid

126 RpiB-specific leads for drug development.

127 **Results**

128 *Li*RpiB recombinant protein was expressed, purified and subjected to thermal shift

129 analysis. Thermal shift (differential scanning fluorimetry) is reliant on fluorescent

130 dyes that signify when a protein has unfolded (21). One of the most commonly used

131 fluorescent dyes is SYPRO® Orange (also used here), which forms non-specific

132 interactions with hydrophobic protein residues (22). This means its signal will be

133 strongest when the protein being analysed is unfolded and internal hydrophobic

134 residues are exposed. By running an assay where reaction temperature is increased

135 in degree increments per minute, it is possible to define the temperature at which a

136 protein unfolds by monitoring its fluorescence. The temperature at which this occurs

137 is designated the protein's (T_m) or melting point (21). Compounds that significantly

138 alter T_m may be potential inhibitors. Initial testing showed *Li*RpiB was amenable to

139 SYPRO® Orange thermal shift analysis, with an average T_m of 59.6°C being

140 obtained for the protein.

141 To permit screening of a fragment library, a positive control for ligand binding had to

142 be established. The obvious choice was the enzyme's substrate: ribose-5-phosphate

143 (R5P). However, reported Km values for R5P against other RpiB enzymes were

144 relatively high, with Stern et al. reporting a R5P Km of 4 mM against *Tc*RpiB (17).

145 Indeed, no significant shifts in *Li*RpiB T_m in the presence of 5-50 mM R5P could be

146 obtained, supporting the suggestion that R5P has a relatively weak interaction with

147 *Li*RpiB and other parasitic RpiBs.

148

7

149   It was hypothesised that 2-deoxyribose-5-phosphate (dR5P) may serve as an

150   alternative, as it could be sufficiently similar to R5P to bind LiRpiB but also be

151   retained in the enzyme's active site for longer, prolonging the interaction. Testing a

152   gradient of dR5P against LiRpiB (5-50 mM) resulted in significant shifts in LiRpiB T_m.

153   To provide the consistency across replicates that would provide Z-factor values for

154   each plate above the confidence threshold (Z-factor > 0.5), 30 mM was selected as

155   the dR5P concentration for positive control reactions, reproducibly inducing a 6 °C

156   shift in LiRpiB T_m (Figure 2).

157

158   Approximately 800 fragments (Figure S2) across 11 fragment plates (Z-factors

159   ranging from 0.5 – 0.8) (Figure S3), were screened at 1 mM effective concentration

160   against LiRpiB. Graphs to summarise the data output for each fragment plate were

161   compiled, with change in T_m relative to the negative control represented for each

162   individual fragment (Figure S4).

163

164   Upon reviewing the thermal shift data for the fragments, a threshold T_m shift of ± 5°C

165   was set for fragment hit selection. This led to the selection of 15 fragment hits (Table

166   1), which were followed up with enzymatic assays and anti-parasitic activity studies.

167

168   Initially, fragment inhibition was tested in LiRpiB in $vitro$ activity assays. Inhibition

169   was compared to that achieved with the well-established Rpi inhibitor 4-PEH, which

170   was tested at 10 mM concentration against both the forward (R5P -> Ru5P) and

171   reverse (Ru5P -> R5P) isomerisation reactions (Table 2). Fragments 328 and 458

172   were excluded from these assays due to solubility problems. To assess whether

173   fragments could be tested in the forward reaction assay, their absorbance at 290 nm

8

174   (0.5 mM and 1 mM concentration) was measured. Almost all fragments displayed

175   high absorbance values at 290 nm (OD ≥ 1) (Figure S5). Therefore, they could not

176   be tested in the forward Rpi activity assay.

177   Only fragments 2, 3, 25, 372, 540 and 576 were tested in this assay. Results for

178   fragment 540 were also excluded during posterior analysis as, in the presence of

179   R5P, the measured signal became saturated, which hindered a clear interpretation of

180   the measurements obtained. Percentage inhibition values for *Li*RpiB that could be

181   determined from the forward Rpi assay are shown (Table 2). No significant inhibition

182   was found through this assay system except in the case of fragment 576: 1 mM 576

183   inhibited the forward reaction to a similar extent as 10 mM 4-PEH (Figure 3). This

184   suggests that 576 is (at least) as potent an inhibitor of *Li*RpiB as 4-PEH.

185

186   The experimental limitations of the forward reaction assay do not apply to the

187   reverse reaction assay. Therefore, all compounds could be tested in the reverse

188   reaction assay system. Fragments 2, 338, 372 and 540 (1 mM) were capable of

189   inhibiting the enzyme to a similar level as 10 mM 4-PEH (Table 2). Surprisingly, the

190   inhibitory capacity of fragment 576 and 4-PEH were not as high in this assay system.

191   This may be due to kinetoplastid RpiB activity favouring production of R5P, meaning

192   higher levels of these inhibitors may be required in order to inhibit the enzyme in this

193   direction.

194

195   The 15 fragment hits and 4-PEH were also tested for their ability to inhibit *L.*

196   *infantum* parasite growth at 100 µM concentration. Compounds were assayed

197   against both *L. infantum* promastigotes (wild-type and *Li*RpiB sKO) and intra-

198   macrophagic amastigotes (Table 2). As 4-PEH is only an inhibitor of LiRpiB at high

199   millimolar range in protein activity assays (10 mM was routinely used to achieve

200   inhibition during this study), it had been anticipated to show little to no anti-parasitic

201   activity *in vitro/in vivo* (7), which was shown to be the case in treating with 100 µM.

202   However, several of the fragment hits were shown to inhibit parasite growth at this

203   concentration. Interestingly, fragments 152, 278 and 540 were seemingly less

204   effective against the LiRpiB sKO promastigotes than the wild-type. Although sKO

205   modifications against essential genes often do not produce significant phenotypic

206   distinctions from wild-type parasites, it's possible that compensatory up-regulation

207   mechanisms accounting for the loss of a single *Li*RpiB allele are acting to protect the

208   parasites from treatment with these compounds (to some extent). Conversely,

209   fragment 576 was active against *Li*RpiB sKO promastigotes but was inactive against

210   the wild-type. As the *in vitro* enzyme assay results point to fragment 576 being a

211   more effective inhibitor of the *Li*RpiB forward reaction than the reverse reaction, this

212   could indicate sKO parasites are rendered more susceptible to forward reaction

213   inhibitors. The most active fragments against both *L-infantum* life-cycle forms were

214   338 (Figure 4) and 540, which were also among the most potent inhibitors of the

215   *Li*RpiB reverse reaction. Collectively, these data suggest that a possible mode of

216   action for the observed anti-leishmanial activity of potent fragments, such as 338, is

217   by modulating the activity of *Li*RpiB.

218

219   To facilitate further development of inhibitor leads, a crystal structure for apo *Li*RpiB

220   was determined at 1.6 Å resolution (Table 3). An *Li*RpiB functional dimer was

221   established, and a *Li*RpiB tetramer could then be assembled from the monomer of

10

222   the asymmetric unit via crystallographic symmetry (Figure 5). This is similar to the

223   TcRpiB tetramer described by Stern et al (16).

224

225   Each monomer of the dimer (hence also of the tetramer) is based on a Rossmann

226   fold with a five-stranded parallel β-sheet flanked by three α-helices on one side and

227   two on the other. A sixth α-helix (C-terminus) extends from the core domain to

228   interact with the second subunit of the dimer. Each monomer subunit of the dimer

229   forms one side of the active site cleft. Within the active site (Figure 6), key residues

230   involved in substrate interaction that have been identified in RpiB homologues are

231   conserved: Asp13, His14, Cys72, Thr74 and Arg116 from one subunit of the dimer

232   and His105, Asn106, Arg140 and Arg144 from the other subunit of the dimer. This

233   indicates the catalytic mechanism operated by the active site is consistent with other

234   RpiBs.

235

236   In comparison to the apo *Tc*RpiB structure, a different orientation of Arg 116 (Arg113

237   in *Tc*RpiB) is observed (Figure 6). Also, Thr74 is present in *Li*RpiB in place of Ser71

238   that occurs in *Tc*RpiB, more in line with *E. coli* RpiB that also carries a Thr residue at

239   this position (11, 16).

240

241   Given the orientation of the sulfate ion in the active site, and the consequent

242   suggestion that the R5P/Ru5P substrate will be oriented in a similar way (Figure 7A),

243   this also indicates 4-PEH interaction with *Li*RpiB will be consistent with that

244   established for other RpiBs (Figure 7B). Docking analysis predictions for anti-

245   parasitic fragment hits 338 and 540 indicates that the interaction of these fragments

246   with the active site are likely to centre around residues His 14, Arg140, Arg144

11

247   (Figure 7C and 7D). Given these residues are conserved in RpiB active sites but not

248   RpiAs, this could account for the selectivity of these fragments towards combatting

249   parasites (Table 2).

250

251

252 **Discussion**

253   Type B ribose-5-phosphate isomerase (RpiB) has been flagged as an attractive

254   protein target for drug development to combat pathogens, given the critical role of

255   this enzyme combined with its evolutionary divergence from mammalian RpiA. It has

256   long been assumed it may be possible to design RpiB specific inhibitors yet, thus far,

257   no such inhibitors have been identified.

258   In this work, a fragment library screening was conducted for *L. infantum* RpiB,

259   utilising thermal shift as the screening technique. Thermal shift assaying is

260   commonly used to assess the potential of adding ligands to improve protein stability,

261   aiding crystallization (21, 23, 24). Although not capable of identifying inhibitors

262   directly, it has been widely used to facilitate this process (25–28), assisting in drug

263   discovery efforts. The ability to apply this screening method to any amenable protein,

264   regardless of function, makes thermal shift particularly valuable. This is perhaps

265   most relevant when attempting to establish inhibitors for proteins that lack high-

266   throughput activity-based screening methods, as was the case for *Li*RpiB. Using this

267   method, *Li*RpiB was screened against 851 different fragments. 15 hit fragments that

268   produced ± 5 °C shifts in *Li*RpiB T_m were selected, progressing to *Li*RpiB activity

269   assays and cell viability assays against *L. infantum* parasites. The activity assay

270   results indicate that thermal shift screening was capable of identifying inhibitors as

271   fragments 2, 338, 372, 540 and 576 showed *Li*RpiB inhibitory activity. Significantly,

272   fragment hits 338 and 540 that inhibited *Li*RpiB *in vitro* also displayed anti-parasitic

273   activity towards both *L. infantum* promastigotes (wild-type and *Li*RpiB sKO) and

274   intramacrophagic amastigotes in an infection model, whilst also being well tolerated

275   by mammalian THP1 cells in cytotoxicity assays. Overall, fragment 338 was

276   considered the best hit against *Li*RpiB given its superior potency. The fact that ability

277   to interact with and inhibit *Li*RpiB was utilised to identify anti-parasitic hits

278   strengthens the case for describing *Li*RpiB as a potential chemically validated drug

279   target in *Leishmania infantum*. This is an important observation given the potential

280   value of RpiB as a drug target in parasitic protozoa has formerly been deemed

281   equivocal (6). Though not specifically examined in this study, the fact RpiB is highly

282   conserved amongst *Leishmania* spp. makes it possible these findings could also

283   apply to species beyond *L. infantum*.

284

285   Previous research into RpiB has largely focused on understanding the enzyme's

286   reaction mechanism, particularly in comparison to RpiA, crystal structure elucidation

287   and/or *in silico* docking studies. Notably, in the context of protozoan parasites,

288   although the crystal structure established for *T. cruzi* RpiB has permitted

289   computational ligand docking studies, potential hits have yet to have their anti-

290   parasitic properties confirmed (20). For many years, inhibition of Rpi has centred

291   around the well-established inhibitor 4-PEH. However, low potency and lack of RpiB

292   specificity render this compound inappropriate for chemotherapeutic applications.

293   The inhibitory fragments reported here, several of which were markedly more potent

294   than 4-PEH (1 mM fragment concentration was contrasted with 10 mM 4-PEH

295   inhibitory activity), may be able to fill this void and provide initial scaffolds for

296   structure-led rational optimisation of RpiB inhibitors. In the case of leishmania, the

297   first crystal structures for a leishmanial RpiB, solved during this study, can greatly

298   facilitate this process for *L. infantum* and other *Leishmania* spp..The structural

299   resolution of *Li*RpiB indicates that, as might be anticipated from high levels of protein

300   sequence homology, RpiB structure is highly conserved amongst protozoan

301 parasites. Thus, there is potential for the design of inhibitors capable of inter-

302 kinetoplastid impact. Docking results for hit anti-parasitic fragments 540 and 338

303 predict that their interaction with the active site of *Li*RpiB hinges on residues His 14,

304 Arg 140 and Arg 144. These residues typically coordinate the phosphate moiety of

305 substrate R5P, orienting and stabilising the substrate in the correct conformation for

306 isomerisation. Thus, it's possible fragments 540 and 338 compete with R5P in the

307 binding of these key residues. Future co-crystallisation and/or structural modelling of

308 the fragments (and, potentially, further analogues) with *Li*RpiB may shed further light

309 on the RpiB catalytic mechanism but also, crucially, how to gain inhibitor specificity

310 over RpiA. It will also be important to establish how the anti-parasitic fragment hits

311 are turned over by the parasites, as currently speculations can only be made as to

312 how intact fragment compounds could interact with *Li*RpiB.

313 Furthermore, it is currently unknown whether any off-target effects are also

314 contributing to fragment efficacy, which will be important to determine going forward,

315 as well as anti-parasitic efficacy towards other *Leishmania* spp.. Overall, however,

316 this work provides new avenues to pursue RpiB as a druggable target in *Leishmania*

317 spp. and other pathogenic organisms.

318

319 **Material and Methods**

320

321 *Cloning of the LiRpiB gene*

322

323 The *Li*RpiB gene was PCR amplified from *L. infantum* genomic DNA

324 (MHOM/MA/67/ITMAP-263), using the following primers: 5'-

325 CAATTTCCATATGCCGAAGCGTGTTGC-3' and 5'-

15

326   CCCAAGCGAATTCTCTACTTTCCTTCC-3'. The purified *Li*RpiB PCR product was

327   NdeI/EcoRI digested and cloned into a pGEM-T Easy vector (Promega). Presence of

328   the *Li*RpiB open-reading frame (ORF) was confirmed via sequencing and was

329   subsequently subcloned into a pET28a(+) expression vector (Novagen).

330   *Expression and purification of recombinant LiRpiB*

331

332   The pET28a(+) *Li*RpiB expression vector was transformed into *E. coli* BL21 (DE3)

333   cells. The recombinant protein was expressed by induction of log-phase cultures in

334   Luria-Bertani media (O$D600$ = 0.6) with 0.5 mM isopropyl-β-D-thiogalactopyranoside

335   (IPTG) for 3 h at 37ºC with shaking at 250 rpm/ min. Bacteria were harvested

336   through centrifugation (3077 g for 40 min at 4ºC) and suspended in 20 mL of buffer A

337   (0.5 M NaCl, 20 mM Tris-HCl, pH 7.6). Samples were then sonicated using a

338   Branson sonifier 250 under the following conditions: output 4, duty cycle 50%, 10

339   cycles with 15 sec each. Samples were centrifuged (3077 g for 60 min at 4ºC) and

340   the product supernatant was retained for further processing. Recombinant *Li*RpiB

341   was purified in one step using Ni^{2+} resin (ProBond), pre-equilibrated in buffer A. The

342   column was washed sequentially with 2-3 mL of the buffer A, 20 ml of the bacterial

343   crude extract, 2 mL of buffer A 25 mM imidazole, 2 mL of buffer A 30 mM imidazole,

344   2 x 2 mL of buffer A 40 mM imidazole, 2 mL of buffer A 50 mM imidazole, 10 mL of

345   buffer A 100 mM imidazole, 5 mL of buffer A 500 mM imidazole and 8 ml of buffer B

346   (1 M imidazole, 0.5 M NaCl, 200 mM Tris, pH 7.6). *Li*RpiB enzyme was eluted in the

347   fractions of buffer A containing 100 or 500 mM of imidazole. Desalting was

348   performed against 100 mM of Tris-HCl, pH 7.6 (storage buffer, reaction buffer for

349   direct reaction), using PD-10 Desalting columns (GE Healthcare Code No 17-0851-

350   01).

351

352   *Differential scanning fluorimetry with LiRpiB*

353

354   Differential scanning fluorimetry was set up in 96-well PCR plates employing a total

355   reaction volume of 100 µL. Reactions consisted of 13 µM protein (*Li*RpiB) in 50 mM

356   MOPs (pH 8.0) reaction buffer with 5 X SYPRO Orange dye (Invitrogen) as the

357   fluorescent indicator of protein unfolding (Ex. 492 nm, Em. 610 nm). Fragments from

358   an in-house library at the University of St Andrews, expanded from the Maybridge

359   Rule of 3 (Ro3) library (25) were screened against RpiB at 1 mM concentration

360   (0.5% DMSO final concentration per well). This library incorporates fragments that

361   adhere to the chemical parameters ≤ 300 MW; ≤ 3.0 cLogP; ≤ 3 H-bond acceptors; ≤

362   3 H-bond donors; ≤ 3 rotatable bonds; ≤ 60 Å^2 Polar Surface Area, properties which

363   are predicted to increase the probability of viable fragment lead discovery (29), a

364   more stringent application of the 'Rule of 5' criteria developed by Lipinski et al. to

365   curate drug-like compound libraries (30). DMSO was used in negative control

366   reactions and 30 mM deoxy-ribose-5-phosphate (dR5P) was added to positive

367   control reactions. Each plate screened included 8-replicate negative and 8-replicate

368   positive control reactions, to permit calculation of a Z-factor (31) (threshold = 0.5).

369   Thermal shift scans were performed in a real-time PCR machine (Stratagene

370   Mx3005P with software MxPro v 4.01) over a temperature range of 25°C to 95°C,

371   ramping at 0.5°C min^{-1}. Data were then exported to Excel for analysis using "DSF

372   analysis", modified from the template provided by Niesen et al (21). Melting point

373   (T_m) values were calculated through non-linear regression analysis, fitting the

374   Boltzmann equation to denaturation curves using GraphPad Prism as previously

375   described (25).

376

377   *Compound preparation for assays*

378

379   Compounds were dissolved in 100% DMSO at 100 mM, aliquoted and stored at -

380   20°C. The following procedure was applied for the solubilization of compounds in

381   reaction buffer (100 mM Tris-HCl pH 7.6): 1 hour of vortex mixing, 15 minutes of

382   ultrasound treatment and 1 hr of incubation at 37°C under strong agitation. The

383   optical density (OD) at 290 nm of soluble compounds at 1 mM or 0.5 mM

384   concentration was measured and only compounds with low absorbance values (OD

385   < 1) were selected for analysis. The control compound 4-PEH was used as a 100

386   mM stock in water and stored at -20ºC.

387

388   *LiRpiB activity assays*

389

390   Compounds were tested in the forward and/or reverse reaction at a final

391   concentration of 1 mM. Concerning the forward reaction, a direct spectrophotometric

392   method at 290 nm was used to quantify Ru5P formation in the presence of 12.5 mM

393   R5P and 0.0025 mg/ml *Li*RpiB in a total volume of 300 µL (32). The reaction buffer

394   was 100 mM of Tris-HCl pH 7.6. The absorbance was monitored at 37°C for 20

395   minutes. The blank for each compound was assumed to be the absorbance at t=0.

396   Compound inhibitory effect was quantified via measuring OD values in both the

397   presence and absence of compound within the first 4 minutes of the assay and at the

398   endpoint (t=20). The ratio between these values were used to determine compound

399   percentage (%) inhibition. In the inverse reaction, a modification of Dische's

400   Cysteine-Carbazole method was used to quantify R5P formation (17). In a total

401 volume of 15 µL, 5 mM Ru5P, 0.0025 mg/mL *Li*RpiB and 5 µL of compound were

402 incubated for 10 minutes at room temperature. Reaction buffer was 100 mM Tris-

403 HCl, 1 mM EDTA and 0.5 mM 2-mercaptoethanol, pH 8.4. For colour revelation, 15

404 µL of 0.5% cysteinium chloride, 125 µL of 75% (v/v) sulfuric acid and 5 µl of a 0.1%

405 solution of carbazole in ethanol were added to 10 µl of the previous mixture. The

406 absorbance at 546 nm was determined following incubation for 30 minutes at room

407 temperature in the dark. A blank without enzyme was always run in tandem with and

408 without compound). The enzyme activity in the presence of compounds was

409 measured by subtracting the OD values obtained in the presence of the enzyme to

410 the blank values. Percentage inhibition was assessed via normalization of the activity

411 values against those obtained in the compound negative control reactions.

412

413 *Parasite culture*

414

415 *L. infantum* (MHOM/MA/67/ITMAP-263) wild-type promastigotes and single knockout

416 (sKO) *Li*RpiB promastigotes (19) were maintained at 27ºC in complete RPMI

417 1640(33). Axenic amastigotes of the same strain expressing firefly luciferase (34)

418 were grown at 37ºC with 5% CO2 in a cell-free medium (35).

419

420 *Growth inhibition assays*

421

422 The percentage growth inhibition, in promastigotes was performed by incubating the

423 parasites in a 96-well plate with a starting inoculum of 1×10^{6} cells/ml promastigotes

424 during 72 hours with defined concentrations of the selected fragments. After

425 incubation 50 µM of resazurin was added and incubated for 4 h. Fluorescence was

426   measured at 540 nm and 620 nm excitation and emission wavelength, respectively,

427   using a Synergy 2 Multi-Mode Reader (Biotek). Activity against intracellular

428   amastigotes was measured using THP1 cells infected with luciferase-expressing

429   amastigotes as previously described (36). Fragments were screened at 100 µM in

430   these assays. THP1 cytotoxicity was determined using an MTT assay following

431   exposure of the THP1 cells to 100 µM of the fragments, as described elsewhere

432   (37).

433

434   *Production and purification of LiRpiB for crystallization*

435

436   The purification protocol was based on that of *Tc*RpiB (17). Briefly, full-length *Li*RpiB

437   was produced as described above except that expression was induced overnight at

438   18°C with 0.7 mM IPTG. Cells were harvested via centrifugation (2500 g for 30 min

439   at 4ºC) and stored at -20°C until use. After thawing, bacterial pellets were suspended

440   in lysis buffer (50 mM Tris.HCl pH 7.5, 300 mM NaCl, 1 mM DTT and 20 mM

441   imidazole). Following sonication, the cell homogenate was centrifuged (56000 g for

442   30 min at 4ºC) and the soluble tagged protein was purified by affinity

443   chromatography on His60 Ni Superflow Resin (Clontech). Lysis buffer was used to

444   wash the resin and protein was eluted with buffer A (50 mM Tris.HCl pH 7.5, 300 mM

445   NaCl, 1 mM DTT and 500 mM imidazole). After removal of the His-tag (thrombin

446   cleavage - overnight, 4°C), additional SEC was carried out on a HiLoad 16/60

447   Superdex 200 equilibrated with buffer B (20 mM Tris.HCl pH 7.5, 150 mM NaCl, 2

448   mM DTT and 1 mM EDTA). Fractions containing purified protein were pooled and

449   protein was concentrated to ~12 mg/ml by ultrafiltration.

450

451 *Crystallization and data collection*

452

453 Crystallization experiments were carried out using the sitting drop vapor diffusion

454 method in 96-well plates using an Innovadyne nanodrop robot (300 nl protein

455 solution + 300 nl crystallization condition). *Li*RpiB crystals grew at 277K in 100 mM

456 HEPES (pH 7) and 2 M ammonium sulfate. Crystals were flash-frozen in liquid

457 nitrogen in crystallization condition supplemented with 22% glycerol. Diffraction data

458 were collected on beamline Proxima 1 (SOLEIL, Saclay, France) on a Pilatus 6M

459 detector.

460

461 *Structure determination and refinement*

462

463 X-ray data were processed with XDS (38) and the software package CCP4 (39). The

464 *Li*RpiB structure was solved by molecular replacement with Phaser (40, 41) using

465 *Tc*RpiB (Protein Data Bank entry code 3K7O) (16) as the search model. Model

466 building and improvement were conducted by iterative cycles of manual building with

467 Coot (42) and refinement with REFMAC (43). Structural data has been deposited in

468 the Protein Data Bank under entry code 6FXW.

469

470 *In silico docking analysis*

471

472 Docking analysis was conducted using PyRx. Ligands (PEH and fragments 338 and

473 540) were prepared using Chem3D, using the package's MM2 structure optimisation

474 tool. The *Li*RpiB functional dimer was prepared as a macromolecule for docking

475 using AutoDock Tools (44, 45). PyRx docking analysis (46) was performed using a

21

476 grid box with dimensions x = 9.217; y = 9.292 and z = 11.459 to encompass the

477 enzyme's active site, determining the ligand conformations that would provide

478 optimal binding energies (exhaustiveness = 16), which were then studied in relation

479 to the *Li*RpiB active site structure using PyMOL.

480

481 **Acknowledgements**

489

490 **References**

491 1. James SL, Abate D, Abate KH, Abay SM, Abbafati C, Abbasi N, Abbastabar H,

492 Abd-Allah F, Abdela J, Abdelalim A, Abdollahpour I, Abdulkader RS, Abebe Z,

493 Abera SF, Abil OZ, Abraha HN, Abu-Raddad LJ, Abu-Rmeileh NME,

494 Accrombessi MMK, Acharya D, Acharya P, Ackerman IN, Adamu AA, Adebayo

495 OM, Adekanmbi V, Adetokunboh OO, Adib MG, Adsuar JC, Afanvi KA,

496 Afarideh M, Afshin A, Agarwal G, Agesa KM, Aggarwal R, Aghayan SA,

497 Agrawal S, Ahmadi A, Ahmadi M, Ahmadieh H, Ahmed MB, Aichour AN,

498 Aichour I, Aichour MTE, Akinyemiju T, Akseer N, Al-Aly Z, Al-Eyadhy A, Al-

499 Mekhlafi HM, Al-Raddadi RM, Alahdab F, Alam K, Alam T, Alashi A, Alavian

500 SM, Alene KA, Alijanzadeh M, Alizadeh-Navaei R, Aljunid SM, Alkerwi A, Alla

501   F, Allebeck P, Alouani MML, Altirkawi K, Alvis-Guzman N, Amare AT, Aminde

502   LN, Ammar W, Amoako YA, Anber NH, Andrei CL, Androudi S, Animut MD,

503   Anjomshoa M, Ansha MG, Antonio CAT, Anwari P, Arabloo J, Arauz A, Aremu

504   O, Ariani F, Armoon B, Ärnlöv J, Arora A, Artaman A, Aryal KK, Asayesh H,

505   Asghar RJ, Ataro Z, Atre SR, Ausloos M, Avila-Burgos L, Avokpaho EFGA,

506   Awasthi A, Ayala Quintanilla BP, Ayer R, Azzopardi PS, Babazadeh A, Badali

507   H, Badawi A, Bali AG, Ballesteros KE, Ballew SH, Banach M, Banoub JAM,

508   Banstola A, Barac A, Barboza MA, Barker-Collo SL, Bärnighausen TW,

509   Barrero LH, Baune BT, Bazargan-Hejazi S, Bedi N, Beghi E, Behzadifar M,

510   Behzadifar M, Béjot Y, Belachew AB, Belay YA, Bell ML, Bello AK, Bensenor

511   IM, Bernabe E, Bernstein RS, Beuran M, Beyranvand T, Bhala N, Bhattarai S,

512   Bhaumik S, Bhutta ZA, Biadgo B, Bijani A, Bikbov B, Bilano V, Bililign N, Bin

513   Sayeed MS, Bisanzio D, Blacker BF, Blyth FM, Bou-Orm IR, Boufous S,

514   Bourne R, Brady OJ, Brainin M, Brant LC, Brazinova A, Breitborde NJK,

515   Brenner H, Briant PS, Briggs AM, Briko AN, Britton G, Brugha T, Buchbinder

516   R, Busse R, Butt ZA, Cahuana-Hurtado L, Cano J, Cárdenas R, Carrero JJ,

517   Carter A, Carvalho F, Castañeda-Orjuela CA, Castillo Rivas J, Castro F,

518   Catalá-López F, Cercy KM, Cerin E, Chaiah Y, Chang AR, Chang HY, Chang

519   JC, Charlson FJ, Chattopadhyay A, Chattu VK, Chaturvedi P, Chiang PPC,

520   Chin KL, Chitheer A, Choi JYJ, Chowdhury R, Christensen H, Christopher DJ,

521   Cicuttini FM, Ciobanu LG, Cirillo M, Claro RM, Collado-Mateo D, Cooper C,

522   Coresh J, Cortesi PA, Cortinovis M, Costa M, Cousin E, Criqui MH, Cromwell

523   EA, Cross M, Crump JA, Dadi AF, Dandona L, Dandona R, Dargan PI, Daryani

524   A, Das Gupta R, Das Neves J, Dasa TT, Davey G, Davis AC, Davitoiu DV, De

525   Courten B, De La Hoz FP, De Leo D, De Neve JW, Degefa MG, Degenhardt L,

23

526   Deiparine S, Dellavalle RP, Demoz GT, Deribe K, Dervenis N, Des Jarlais DC,

527   Dessie GA, Dey S, Dharmaratne SD, Dinberu MT, Dirac MA, Djalalinia S,

528   Doan L, Dokova K, Doku DT, Dorsey ER, Doyle KE, Driscoll TR, Dubey M,

529   Dubljanin E, Duken EE, Duncan BB, Duraes AR, Ebrahimi H, Ebrahimpour S,

530   Echko MM, Edvardsson D, Effiong A, Ehrlich JR, El Bcheraoui C, El Sayed

531   Zaki M, El-Khatib Z, Elkout H, Elyazar IRF, Enayati A, Endries AY, Er B,

532   Erskine HE, Eshrati B, Eskandarieh S, Esteghamati A, Esteghamati S, Fakhim

533   H, Fallah Omrani V, Faramarzi M, Fareed M, Farhadi F, Farid TA, Farinha

534   CSE, Farioli A, Faro A, Farvid MS, Farzadfar F, Feigin VL, Fentahun N,

535   Fereshtehnejad SM, Fernandes E, Fernandes JC, Ferrari AJ, Feyissa GT, Filip

536   I, Fischer F, Fitzmaurice C, Foigt NA, Foreman KJ, Fox J, Frank TD, Fukumoto

537   T, Fullman N, Fürst T, Furtado JM, Futran ND, Gall S, Ganji M, Gankpe FG,

538   Garcia-Basteiro AL, Gardner WM, Gebre AK, Gebremedhin AT, Gebremichael

539   TG, Gelano TF, Geleijnse JM, Genova-Maleras R, Geramo YCD, Gething PW,

540   Gezae KE, Ghadiri K, Ghasemi Falavarjani K, Ghasemi-Kasman M, Ghimire

541   M, Ghosh R, Ghoshal AG, Giampaoli S, Gill PS, Gill TK, Ginawi IA, Giussani

542   G, Gnedovskaya E V., Goldberg EM, Goli S, Gómez-Dantés H, Gona PN,

543   Gopalani SV, Gorman TM, Goulart AC, Goulart BNG, Grada A, Grams ME,

544   Grosso G, Gugnani HC, Guo Y, Gupta PC, Gupta R, Gupta R, Gupta T,

545   Gyawali B, Haagsma JA, Hachinski V, Hafezi-Nejad N, Haghparast Bidgoli H,

546   Hagos TB, Hailu GB, Haj-Mirzaian A, Haj-Mirzaian A, Hamadeh RR, Hamidi S,

547   Handal AJ, Hankey GJ, Hao Y, Harb HL, Harikrishnan S, Haro JM, Hasan M,

548   Hassankhani H, Hassen HY, Havmoeller R, Hawley CN, Hay RJ, Hay SI,

549   Hedayatizadeh-Omran A, Heibati B, Hendrie D, Henok A, Herteliu C,

550   Heydarpour S, Hibstu DT, Hoang HT, Hoek HW, Hoffman HJ, Hole MK,

551 Homaie Rad E, Hoogar P, Hosgood HD, Hosseini SM, Hosseinzadeh M,

552 Hostiuc M, Hostiuc S, Hotez PJ, Hoy DG, Hsairi M, Htet AS, Hu G, Huang JJ,

553 Huynh CK, Iburg KM, Ikeda CT, Ileanu B, Ilesanmi OS, Iqbal U, Irvani SSN,

554 Irvine CMS, Mohammed S, Islam S, Islami F, Jacobsen KH, Jahangiry L,

555 Jahanmehr N, Jain SK, Jakovljevic M, Javanbakht M, Jayatilleke AU, Jeemon

556 P, Jha RP, Jha V, Ji JS, Johnson CO, Jonas JB, Jozwiak JJ, Jungari SB,

557 Jürisson M, Kabir Z, Kadel R, Kahsay A, Kalani R, Kanchan T, Karami M,

558 Karami Matin B, Karch A, Karema C, Karimi N, Karimi SM, Kasaeian A, Kassa

559 DH, Kassa GM, Kassa TD, Kassebaum NJ, Katikireddi SV, Kawakami N,

560 Kazemi Karyani A, Keighobadi MM, Keiyoro PN, Kemmer L, Kemp GR,

561 Kengne AP, Keren A, Khader YS, Khafaei B, Khafaie MA, Khajavi A, Khalil IA,

562 Khan EA, Khan MS, Khan MA, Khang YH, Khazaei M, Khoja AT, Khosravi A,

563 Khosravi MH, Kiadaliri AA, Kiirithio DN, Kim C II, Kim D, Kim P, Kim YE, Kim

564 YJ, Kimokoti RW, Kinfu Y, Kisa A, Kissimova-Skarbek K, Kivimäki M, Knudsen

565 AKS, Kocarnik JM, Kochhar S, Kokubo Y, Kolola T, Kopec JA, Kosen S,

566 Kotsakis GA, Koul PA, Koyanagi A, Kravchenko MA, Krishan K, Krohn KJ,

567 Kuate Defo B, Kucuk Bicer B, Kumar GA, Kumar M, Kyu HH, Lad DP, Lad SD,

568 Lafranconi A, Lalloo R, Lallukka T, Lami FH, Lansingh VC, Latifi A, Lau KMM,

569 Lazarus J V., Leasher JL, Ledesma JR, Lee PH, Leigh J, Leung J, Levi M,

570 Lewycka S, Li S, Li Y, Liao Y, Liben ML, Lim LL, Lim SS, Liu S, Lodha R,

571 Looker KJ, Lopez AD, Lorkowski S, Lotufo PA, Low N, Lozano R, Lucas TCD,

572 Lucchesi LR, Lunevicius R, Lyons RA, Ma S, Macarayan ERK, Mackay MT,

573 Madotto F, Magdy Abd El Razek H, Magdy Abd El Razek M, Maghavani DP,

574 Mahotra NB, Mai HT, Majdan M, Majdzadeh R, Majeed A, Malekzadeh R,

575 Malta DC, Mamun AA, Manda AL, Manguerra H, Manhertz T, Mansournia MA,

576   Mantovani LG, Mapoma CC, Maravilla JC, Marcenes W, Marks A, Martins-

577   Melo FR, Martopullo I, März W, Marzan MB, Mashamba-Thompson TP,

578   Massenburg BB, Mathur MR, Matsushita K, Maulik PK, Mazidi M, McAlinden

579   C, McGrath JJ, McKee M, Mehndiratta MM, Mehrotra R, Mehta KM, Mehta V,

580   Mejia-Rodriguez F, Mekonen T, Melese A, Melku M, Meltzer M, Memiah PTN,

581   Memish ZA, Mendoza W, Mengistu DT, Mengistu G, Mensah GA, Mereta ST,

582   Meretoja A, Meretoja TJ, Mestrovic T, Mezerji NMG, Miazgowski B,

583   Miazgowski T, Millear AI, Miller TR, Miltz B, Mini GK, Mirarefin M, Mirrakhimov

584   EM, Misganaw AT, Mitchell PB, Mitiku H, Moazen B, Mohajer B, Mohammad

585   KA, Mohammadifard N, Mohammadnia-Afrouzi M, Mohammed MA,

586   Mohammed S, Mohebi F, Moitra M, Mokdad AH, Molokhia M, Monasta L,

587   Moodley Y, Moosazadeh M, Moradi G, Moradi-Lakeh M, Moradinazar M,

588   Moraga P, Morawska L, Moreno Velásquez I, Morgado-Da-Costa J, Morrison

589   SD, Moschos MM, Mousavi SM, Mruts KB, Muche AA, Muchie KF, Mueller

590   UO, Muhammed OS, Mukhopadhyay S, Muller K, Mumford JE, Murhekar M,

591   Musa J, Musa KI, Mustafa G, Nabhan AF, Nagata C, Naghavi M, Naheed A,

592   Nahvijou A, Naik G, Naik N, Najafi F, Naldi L, Nam HS, Nangia V, Nansseu

593   JR, Nascimento BR, Natarajan G, Neamati N, Negoi I, Negoi RI, Neupane S,

594   Newton CRJ, Ngunjiri JW, Nguyen AQ, Nguyen HT, Nguyen HLT, Nguyen HT,

595   Nguyen LH, Nguyen M, Nguyen NB, Nguyen SH, Nichols E, Ningrum DNA,

596   Nixon MR, Nolutshungu N, Nomura S, Norheim OF, Noroozi M, Norrving B,

597   Noubiap JJ, Nouri HR, Nourollahpour Shiadeh M, Nowroozi MR, Nsoesie EO,

598   Nyasulu PS, Odell CM, Ofori-Asenso R, Ogbo FA, Oh IH, Oladimeji O,

599   Olagunju AT, Olagunju TO, Olivares PR, Olsen HE, Olusanya BO, Ong KL,

600   Ong SK, Oren E, Ortiz A, Ota E, Otstavnov SS, øverland S, Owolabi MO,

601 Mahesh PA, Pacella R, Pakpour AH, Pana A, Panda-Jonas S, Parisi A, Park

602 EK, Parry CDH, Patel S, Pati S, Patil ST, Patle A, Patton GC, Paturi VR,

603 Paulson KR, Pearce N, Pereira DM, Perico N, Pesudovs K, Pham HQ, Phillips

604 MR, Pigott DM, Pillay JD, Piradov MA, Pirsaheb M, Pishgar F, Plana-Ripoll O,

605 Plass D, Polinder S, Popova S, Postma MJ, Pourshams A, Poustchi H,

606 Prabhakaran D, Prakash S, Prakash V, Purcell CA, Purwar MB, Qorbani M,

607 Quistberg DA, Radfar A, Rafay A, Rafiei A, Rahim F, Rahimi K, Rahimi-

608 Movaghar A, Rahimi-Movaghar V, Rahman M, Ur Rahman MH, Rahman MA,

609 Rahman SU, Rai RK, Rajati F, Ram U, Ranjan P, Ranta A, Rao PC, Rawaf

610 DL, Rawaf S, Reddy KS, Reiner RC, Reinig N, Reitsma MB, Remuzzi G,

611 Renzaho AMN, Resnikoff S, Rezaei S, Rezai MS, Ribeiro ALP, Robinson SR,

612 Roever L, Ronfani L, Roshandel G, Rostami A, Roth GA, Roy A, Rubagotti E,

613 Sachdev PS, Sadat N, Saddik B, Sadeghi E, Saeedi Moghaddam S, Safari H,

614 Safari Y, Safari-Faramani R, Safdarian M, Safi S, Safiri S, Sagar R, Sahebkar

615 A, Sahraian MA, Sajadi HS, Salam N, Salama JS, Salamati P, Saleem K,

616 Saleem Z, Salimi Y, Salomon JA, Salvi SS, Salz I, Samy AM, Sanabria J,

617 Sang Y, Santomauro DF, Santos IS, Santos JV, Santric Milicevic MM, Sao

618 Jose BP, Sardana M, Sarker AR, Sarrafzadegan N, Sartorius B, Sarvi S,

619 Sathian B, Satpathy M, Sawant AR, Sawhney M, Saxena S, Saylan M,

620 Schaeffner E, Schmidt MI, Schneider IJC, Schöttker B, Schwebel DC,

621 Schwendicke F, Scott JG, Sekerija M, Sepanlou SG, Serván-Mori E,

622 Seyedmousavi S, Shabaninejad H, Shafieesabet A, Shahbazi M, Shaheen AA,

623 Shaikh MA, Shams-Beyranvand M, Shamsi M, Shamsizadeh M, Sharafi H,

624 Sharafi K, Sharif M, Sharif-Alhoseini M, Sharma M, Sharma R, She J, Sheikh

625 A, Shi P, Shibuya K, Shigematsu M, Shiri R, Shirkoohi R, Shishani K, Shiue I,

626   Shokraneh F, Shoman H, Shrime MG, Si S, Siabani S, Siddiqi TJ, Sigfusdottir

627   ID, Sigurvinsdottir R, Silva JP, Silveira DGA, Singam NSV, Singh JA, Singh

628   NP, Singh V, Sinha DN, Skiadaresi E, Slepak ELN, Sliwa K, Smith DL, Smith

629   M, Soares Filho AM, Sobaih BH, Sobhani S, Sobngwi E, Soneji SS, Soofi M,

630   Soosaraei M, Sorensen RJD, Soriano JB, Soyiri IN, Sposato LA,

631   Sreeramareddy CT, Srinivasan V, Stanaway JD, Stein DJ, Steiner C, Steiner

632   TJ, Stokes MA, Stovner LJ, Subart ML, Sudaryanto A, Sufiyan MB, Sunguya

633   BF, Sur PJ, Sutradhar I, Sykes BL, Sylte DO, Tabarés-Seisdedos R,

634   Tadakamadla SK, Tadesse BT, Tandon N, Tassew SG, Tavakkoli M, Taveira

635   N, Taylor HR, Tehrani-Banihashemi A, Tekalign TG, Tekelemedhin SW, Tekle

636   MG, Temesgen H, Temsah MH, Temsah O, Terkawi AS, Teweldemedhin M,

637   Thankappan KR, Thomas N, Tilahun B, To QG, Tonelli M, Topor-Madry R,

638   Topouzis F, Torre AE, Tortajada-Girbés M, Touvier M, Tovani-Palone MR,

639   Towbin JA, Tran BX, Tran KB, Troeger CE, Truelsen TC, Tsilimbaris MK, Tsoi

640   D, Tudor Car L, Tuzcu EM, Ukwaja KN, Ullah I, Undurraga EA, Unutzer J,

641   Updike RL, Usman MS, Uthman OA, Vaduganathan M, Vaezi A, Valdez PR,

642   Varughese S, Vasankari TJ, Venketasubramanian N, Villafaina S, Violante FS,

643   Vladimirov SK, Vlassov V, Vollset SE, Vosoughi K, Vujcic IS, Wagnew FS,

644   Waheed Y, Waller SG, Wang Y, Wang YP, Weiderpass E, Weintraub RG,

645   Weiss DJ, Weldegebreal F, Weldegwergs KG, Werdecker A, West TE,

646   Whiteford HA, Widecka J, Wijeratne T, Wilner LB, Wilson S, Winkler AS,

647   Wiyeh AB, Wiysonge CS, Wolfe CDA, Woolf AD, Wu S, Wu YC, Wyper GMA,

648   Xavier D, Xu G, Yadgir S, Yadollahpour A, Yahyazadeh Jabbari SH, Yamada

649   T, Yan LL, Yano Y, Yaseri M, Yasin YJ, Yeshaneh A, Yimer EM, Yip P, Yisma

650   E, Yonemoto N, Yoon SJ, Yotebieng M, Younis MZ, Yousefifard M, Yu C,

651   Zadnik V, Zaidi Z, Zaman S Bin, Zamani M, Zare Z, Zeleke AJ, Zenebe ZM,

652   Zhang K, Zhao Z, Zhou M, Zodpey S, Zucker I, Vos T, Murray CJL. 2018.

653   Global, regional, and national incidence, prevalence, and years lived with

654   disability for 354 Diseases and Injuries for 195 countries and territories, 1990-

655   2017: A systematic analysis for the Global Burden of Disease Study 2017.

656   Lancet 392:1789–1858.

657   2.   Dickie EA, Giordani F, Gould MK, Mäser P, Burri C, Mottram JC, Rao SPS,

658   Barrett MP. 2020. New drugs for human African trypanosomiasis: A twenty first

659   century success story. Trop Med Infect Dis 5:1–15.

660   3.   World Health Organization. 2020. Leishmaniasis. https://www.who.int/news-

661   room/fact-sheets/detail/leishmaniasis. Accessed: 2020-08-06

662   4.   DNDi. 2019. Visceral Leishmaniasis. https://dndi.org/diseases/visceral-

663   leishmaniasis. Accessed: 2020-08-06

664   5.   DNDi. 2020. R&D Portfolio. https://dndi.org/research-development/portfolio.

665   Accessed:2020-08-06.

666   6.   Kovářová J, Barrett MP. 2016. The Pentose Phosphate Pathway in Parasitic

667   Trypanosomatids. Trends Parasitol 32:622–634.

668   7.   Loureiro I, Faria J, Santarem N, Smith TK, Tavares J, Cordeiro-da-Silva A.

669   2018. Potential Drug Targets in the Pentose Phosphate Pathway of

670   Trypanosomatids. Curr Med Chem 25:5239–5265.

671   8.   Stincone A, Prigione A, Cramer T, Wamelink MMC, Campbell K, Cheung E,

672   Olin-Sandoval V, Grüning NM, Krüger A, Tauqeer Alam M, Keller MA,

673   Breitenbach M, Brindle KM, Rabinowitz JD, Ralser M. 2015. The return of

674   metabolism: Biochemistry and physiology of the pentose phosphate pathway.

675   Biol Rev 90:927–963.

676   9.   Essenberg MK, Cooper RA. 1975. Two Ribose-5-Phosphate Isomerases from

677   *Escherichia coli* K12: Partial Characterisation of the Enzymes and

678   Consideration of Their Possible Physiological Roles. Eur J Biochem 55:323–

679   332.

680   10.   Capriles PVSZ, Baptista LPR, Guedes IA, Guimaraes ACR, Custodio FL,

681   Alves-Ferreira M, Dardenne LE. 2015. Structural modeling and docking studies

682   of ribose 5-phosphate isomerase from *Leishmania major* and *Homo sapiens*: A

683   comparative analysis for Leishmaniasis treatment. J Mol Graph Model 55:134–

684   147.

685   11.   Zhang RG, Andersson CE, Skarina T, Evdokimova E, Edwards AM,

686   Joachimiak A, Savchenko A, Mowbray SL. 2003. The 2.2 Å resolution

687   structure of RpiB/AlsB from *Escherichia coli* illustrates a new approach to the

688   ribose-5-phosphate isomerase reaction. J Mol Biol 332:1083–1094.

689   12.   Roos AK, Andersson CE, Bergfors T, Jacobsson M, Karlén A, Unge T, Jones

690   TA, Mowbray SL. 2004. *Mycobacterium tuberculosis* ribose-5-phosphate

691   isomerase has a known fold, but a novel active site. J Mol Biol 335:799–809.

692   13.   Roos AK, Mariano S, Kowalinski E, Salmon L, Mowbray SL. 2008. d-Ribose-5-

693   Phosphate Isomerase B from *Escherichia coli* is Also a Functional d-Allose-6-

694   Phosphate Isomerase, While the *Mycobacterium tuberculosis* Enzyme is Not. J

695   Mol Biol 382:667–679.

696   14.   Roos AK, Burgos E, Ericsson DJ, Salmon L, Mowbray SL. 2005. Competitive

697   inhibitors of *Mycobacterium tuberculosis* ribose-5-phosphate isomerase B

698   reveal new information about the reaction mechanism. J Biol Chem 280:6416–

699   6422.

700   15.   Loureiro I, Faria J, Clayton C, Macedo-Ribeiro S, Santarém N, Roy N,

701   Cordeiro-da-Siva A, Tavares J. 2015. Ribose 5-Phosphate Isomerase B

702   Knockdown Compromises *Trypanosoma brucei* Bloodstream Form Infectivity.

703   PLoS Negl Trop Dis 9:1–11.

704 16. Stern AL, Naworyta A, Cazzulo JJ, Mowbray SL. 2011. Structures of type B

705   ribose 5-phosphate isomerase from *Trypanosoma cruzi* shed light on the

706   determinants of sugar specificity in the structural family. FEBS J 278:793–808.

707 17. Stern AL, Burgos E, Salmon L, Cazzulo JJ. 2007. Ribose 5-phosphate

708   isomerase type B from *Trypanosoma cruzi*: kinetic properties and site-directed

709   mutagenesis reveal information about the reaction mechanism. Biochem J

710   401:279–85.

711 18. Kaur PK, Tripathi N, Desale J, Neelagiri S, Yadav S, Bharatam P V., Singh S.

712   2016. Mutational and structural analysis of conserved residues in ribose-5-

713   phosphate isomerase B from *Leishmania donovani*: Role in substrate

714   recognition and conformational stability. PLoS One 11:1–20.

715 19. Faria J, Loureiro I, Santarem N, Cecilio P, Macedo-Ribeiro S, Tavares J,

716   Cordeiro-da-Silva A. 2016. Disclosing the essentiality of ribose-5-phosphate

717   isomerase B in Trypanosomatids. Sci Rep 6:26937.

718 20. de V. C. Sinatti V, Luiz LP, Alves-Ferreira M, Dardenne L, Hermínio Martins da

719   Silva J, Guimarães AC. 2017. In silico identification of inhibitors of ribose 5-

720   phosphate isomerase from *Trypanosoma cruzi* using ligand and structure

721   based approaches. J Mol Graph Model 77:168–180.

722 21. Niesen FH, Berglund H, Vedadi M. 2007. The use of differential scanning

723   fluorimetry to detect ligand interactions that promote protein stability. Nat

724   Protoc 2:2212–21.

725 22. Hawe A, Sutter M, Jiskoot W. 2008. Extrinsic fluorescent dyes as tools for

726   protein characterization. Pharm Res 25:1487–1499.

727   23.   Alexandrov AI, Mileni M, Chien EYT, Hanson MA, Stevens RC. 2008.

728   Microscale fluorescent thermal stability assay for membrane proteins.

729   Structure 16:351–9.

730   24.   Ericsson UB, Hallberg BM, DeTitta GT, Dekker N, Nordlund P. 2006.

731   Thermofluor-based high-throughput stability optimization of proteins for

732   structural studies. Anal Biochem 357:289–298.

733   25.   Major LL, Smith TK. 2011. Screening the MayBridge Rule of 3 Fragment

734   Library for Compounds That Interact with the *Trypanosoma brucei* myo-

735   Inositol-3-Phosphate Synthase and/or Show Trypanocidal Activity. Mol Biol Int

736   2011:389364.

737   26.   Major LL, Denton H, Smith TK. 2013. Coupled Enzyme Activity and Thermal

738   Shift Screening of the Maybridge Rule of 3 Fragment Library Against

739   *Trypanosoma brucei* Choline Kinase; A Genetically Validated Drug Target, p.

740   413–431. *In* El-Shemy, HA (ed.), Drug Discovery. InTech.

741   27.   Lo M-C, Aulabaugh A, Jin G, Cowling R, Bard J, Malamas M, Ellestad G.

742   2004. Evaluation of fluorescence-based thermal shift assays for hit

743   identification in drug discovery. Anal Biochem 332:153–9.

744   28.   Krishna SN, Luan CH, Mishra RK, Xu L, Scheidt KA, Anderson WF, Bergan

745   RC. 2013. A fluorescence-based thermal shift assay identifies inhibitors of

746   mitogen activated protein kinase kinase 4. PLoS One 8.

747   29.   Carr RAE, Congreve M, Murray CW, Rees DC. 2005. Fragment-based lead

748   discovery: Leads by design. Drug Discov Today 10:987–992.

749   30.   Lipinski CA, Lombardo F, Dominy BW, Feeney PJ. 1997. Experimental and

750   computational approaches to estimate solubility and permeability in drug

751   discovery and development settings. Adv Drug Deliv Rev 23:3–25.

752 31. Zhang J-H, Chung TDY, Oldenburg KR. 1999. A Simple Statistical Parameter

753   for Use in Evaluation and Validation of High Throughput Screening Assays. J

754   Biomol Screen 4:67–73.

755 32. Igoillo-Esteve M, Maugeri D, Stern a L, Beluardi P, Cazzulo JJ. 2007. The

756   pentose phosphate pathway in *Trypanosoma cruzi*: a potential target for the

757   chemotherapy of Chagas disease. An Acad Bras Cienc 79:649–663.

758 33. Moreira D, Santarém N, Loureiro I, Tavares J, Silva AM, Amorim AM, Ouaissi

759   A, Cordeiro-da-Silva A, Silvestre R. 2012. Impact of continuous axenic

760   cultivation in *Leishmania infantum* virulence. PLoS Negl Trop Dis 6:e1469.

761 34. Sereno D, Roy G, Lemesre JL, Papadopoulou B, Ouellette M. 2001. DNA

762   transformation of *Leishmania infantum* axenic amastigotes and their use in

763   drug screening. Antimicrob Agents Chemother 45:1168–73.

764 35. Sereno D, Lemesre JL. 1997. Axenically cultured amastigote forms as an in

765   vitro model for investigation of antileishmanial agents. Antimicrob Agents

766   Chemother 41:972–6.

767 36. Santarém N, Tavares J, Cordeiro-da-Silva A. 2019. In Vitro Infections of

768   Macrophage-Like Cell Lines with *Leishmania infantum* for Drug Screening, p.

769   265–277. *In* .

770 37. Linciano P, Dawson A, Pöhner I, Costa DM, Sá MS, Cordeiro-da-Silva A,

771   Luciani R, Gul S, Witt G, Ellinger B, Kuzikov M, Gribbon P, Reinshagen J, Wolf

772   M, Behrens B, Hannaert V, Michels PAM, Nerini E, Pozzi C, di Pisa F, Landi

773   G, Santarem N, Ferrari S, Saxena P, Lazzari S, Cannazza G, Freitas-Junior

774   LH, Moraes CB, Pascoalino BS, Alcântara LM, Bertolacini CP, Fontana V,

775   Wittig U, Müller W, Wade RC, Hunter WN, Mangani S, Costantino L, Costi MP.

776   2017. Exploiting the 2-Amino-1,3,4-thiadiazole Scaffold To Inhibit

777   *Trypanosoma brucei* Pteridine Reductase in Support of Early-Stage Drug

778   Discovery. ACS omega 2:5666–5683.

779   38.   Kabsch W. 2010. XDS. Acta Crystallogr Sect D Biol Crystallogr 66:125–132.

780   39.   Winn MD, Ballard CC, Cowtan KD, Dodson EJ, Emsley P, Evans PR, Keegan

781   RM, Krissinel EB, Leslie AGW, McCoy A, McNicholas SJ, Murshudov GN,

782   Pannu NS, Potterton EA, Powell HR, Read RJ, Vagin A, Wilson KS. 2011.

783   Overview of the CCP 4 suite and current developments. Acta Crystallogr Sect

784   D Biol Crystallogr 67:235–242.

785   40.   Collaborative Computational Project N 4. 1994. The CCP4 suite: programs for

786   protein crystallography. Acta Crystallogr D Biol Crystallogr 50:760–3.

787   41.   McCoy AJ, Grosse-Kunstleve RW, Adams PD, Winn MD, Storoni LC, Read

788   RJ. 2007. Phaser crystallographic software. J Appl Crystallogr 40:658–674.

789   42.   Emsley P, Lohkamp B, Scott WG, Cowtan K. 2010. Features and development

790   of Coot. Acta Crystallogr D Biol Crystallogr 66:486–501.

791   43.   Murshudov GN, Skubák P, Lebedev AA, Pannu NS, Steiner RA, Nicholls RA,

792   Winn MD, Long F, Vagin AA. 2011. REFMAC 5 for the refinement of

793   macromolecular crystal structures. Acta Crystallogr Sect D Biol Crystallogr

794   67:355–367.

795   44.   Sanner MF. 1999. Python: a programming language for software integration

796   and development. J Mol Graph Model 17:57–61.

797   45.   Morris GM, Huey R, Lindstrom W, Sanner MF, Belew RK, Goodsell DS, Olson

798   AJ. 2009. AutoDock4 and AutoDockTools4: Automated docking with selective

799   receptor flexibility. J Comput Chem 30:2785–91.

800   46.   Dallakyan S, Olson AJ. 2015. Small-Molecule Library Screening by Docking

801   with PyRxMethods in Molecular Biology.

802

803

804

805

806

807   **Figure Legends**

808

809   Figure 1 – Overview of the pentose phosphate pathway (PPP). Both oxidative and

810   non-oxidative branches of the pathway are depicted. Ribose-5-phosphate isomerase

811   (Rpi) is highlighted in bold. G6PDH – glucose-6-phosphate dehydrogenase; 6-PGL;

812   6-phosphogluconolactonase; 6-PGDH – 6-phosphogluconate dehydrogenase; RuPE

813   – Ribulose 5-phosphate epimerase; TKT– transketolase; TAL – transaldolase.

814

815   Figure 2: Confirmation LiRpiB is amenable to thermal shift library screening.

816   Fluorescence profiles for 8 replicate LiRpiB negative control reactions (protein in the

817   absence of any potential ligand) and 8 replicate positive control reactions (LiRpiB in

818   the presence of 30 mM dR5P) are shown. LiRpiB T_m = 59.3 $\pm$ 0.08 °C. The presence

819   of 30 mM dR5P produced a 6 °C T_m shift (LiRpiB T_m = 65.6 $\pm$ 0.11 °C).

820

821   Figure 3: Measurements of LiRpiB activity catalysing the forward reaction in the

822   presence of the fragment 576. Values represent the enzyme activity with (squares)

823   and without (circles) the fragment, and with 4-PEH (triangles). The reaction occurred

824   in the presence of 12.5 mM R5P and 0.0025 mg/ml LiRpiB. Fragment 576 and 4-

825   PEH were tested at 1 mM and 10 mM respectively. The absorbance at 290 nm (OD)

35

826   was measured every 30 seconds during 20 minutes at 37℃. The values obtained

827   with the compound 576 and in the control without the fragment correspond to the

828   mean of duplicates. The values concerning the 4-PEH were obtained from a single

829   enzymatic kinetic reading.

830   Figure 4: Average dose response curves. EC50 and 95% confidence interval for

831   miltefosine (A) and fragment 338 (B) anti-parasitic activity against wild-type (WT) and

832   single knockout (sKO) RpiB promastigotes. The curves represent the merged output

833   from the data of three independent curves.

834

835   Figure 5: Reconstitution of *Li*RpiB structure. The green monomer represents the

836   asymmetric unit and additional copies participating in tetramer formation through

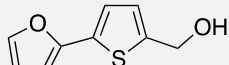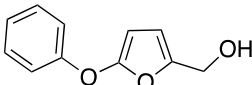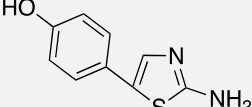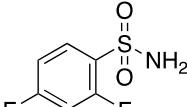837   crystallographic symmetry are depicted in grey.

838
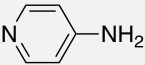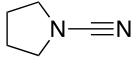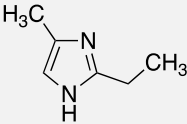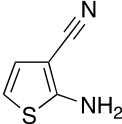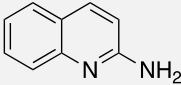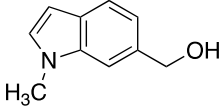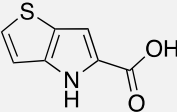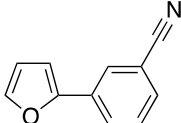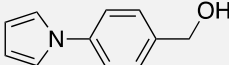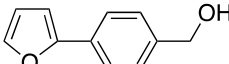
839   Figure 6: *Li*RpiB active site occupied by a sulfate ion. Key residues for *Li*RpiB protein

840   activity are labelled and depicted as sticks, water molecules as red spheres.

841   Conformation of *Tc*RpiB Arg113, as observed in the *Tc*RpiB apo structure, is

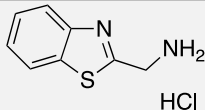842   highlighted in brown transparent stick.

843

844   Figure 7 – *Li*RpiB active site illustrating inhibitor substrate and inhibitor binding

845   predictions. (A) R5P/Ru5P and (B) 4-PEH, predicted with reference to *Tc*RpiB; (C)

846   338 and (D) 540 fragment binding predictions from *in silico* docking analysis. The

847   docking conformations depicted displayed optimal binding energy and highest level

848   of intermolecular interactions.

849

850   Table 1: Fragment hits from thermal shift screening of *Li*RpiB. Fragment library

851   number; name; chemical structure and observed T_m shift (°C) for each fragment hit

852   are provided.

853

Fragment ID	Name	Structure	T_m shift (°C)
2	pyridin-4-amine		12.9
3	pyrrolidine-1-carbonitrile		5.8
25	2-ethyl-4-methyl-1H-imidazole		7.4
68	2-aminothiophene-3-carbonitrile		-9.2
152	quinolin-2-amine		6.6
278	(1-methyl-1H-indol-6-yl)methanol		5.6
328	4H-thieno[3,2-b]pyrrole-5-carboxylic acid		10.4
338	3-(2-furyl)benzonitrile		5.8
372	[4-(1H-pyrrol-1-yl)phenyl]methanol		6.9
383	[4-(2-furyl)phenyl]methanol		9.7
458	[5-(2-furyl)thien-2-yl]methanol		7.6
540	(5-phenoxy-2-furyl)methanol		6.5
565	4-(2-amino-1,3-thiazol-4-yl)phenol		-8.2
576	2,4-difluorobenzenesulfonamide		-8.7

| 626 | 1,3-benzothiazol-2-ylmethylamine hydrochloride | | -6.9 |

854

Table 2: Inhibitory capacity of compounds against *Li*RpiB

The enzymatic inhibition of all the compounds was determined at 1 mM, except the 4-PEH that was tested at 10 mM. The values correspond to the mean +/- SD of the inhibitory effect (%) relative to control (drug absence) from 2-3 independent assays performed in duplicate. The activity of 100 µM of each fragment against *L. infantum* promastigotes was determined using resazurin assay (72 hours). For the intra-macrophagic parasites, THP1 cells infected with parasites expressing luciferase were used. The cytotoxicity and activity determinations were performed with 100 µM of the fragments in a MTT assay involving PMA-differentiated THP-1 cells. Anti-parasite and viability data represented is the average ± SD of at least two independent assays performed in at least triplicate. NA, not active; NT, not tested.

Inhibitor	*Li*RpiB inhibition (%)		Anti-parasitic activity (%)			THP1 viability (%)
	Forward	Reverse	Promastigote WT	Promastigote sKO RpiB	Amastigote	
2	10 ± 14	21 ± 2	N.A.	N.A.	30 ± 8	92 ± 1
3	12 ± 9	10 ± 4	14 ± 5	9 ± 0	79 ± 26	99 ± 3
25	6 ± 1	6 ± 7	N.A.	N.A.	40 ± 31	115 ± 26
68	N.T.	19 ± 1	N.A.	N.A.	N.A.	120 ± 18
152	N.T.	13 ± 8	31 ± 11	52 ± 24	N.A.	114 ± 15
278	N.T.	4 ± 4	13 ± 1	28 ± 5	N.A.	19 ± 1
338	N.T.	32 ± 10	100 ± 0	102 ± 2	100 ± 17	77 ± 14
372	5 ± 15	26 ± 3	N.A.	N.A.	N.A.	96 ± 5
383	N.T.	-2 ± 1	N.A.	N.A.	N.A.	121 ± 16
540	N.T.	23 ± 5	26 ± 15	64 ± 5	87 ± 15	71 ± 2
565	N.T.	17 ± 1	N.A.	N.A.	N.A.	96 ± 0
576	39 ± 22	14 ± 5	N.A.	69 ± 28	N.A.	21 ± 20
626	N.T.	-7 ± 8	N.A.	N.A.	N.A.	101 ± 4
4PEH	51 ± 19	24 ± 4	N.A.	N.A.	N.A.	82 ± 1

866

Table 3. Data collection and refinement statistics

	*Li*RpiB/SO$_4$
Data collection	

Resolution (last shell) (Å)	19.75-1.57 (1.66-1.57)
Space group	F222
Unit-cell parameters	
a, b, c (Å)	a=80.87, b=83.55, c=89.35
α, β, γ (°)	α=β=γ=90
Completeness (last shell) (%)	99.6 (97.8)
Redundancy (%)	6.5
I/σ(I) (last shell)	23.20 (5.09)
Rsym(I) (last shell) (%)	5.27(34.3)
Refinement	
Protein molecule / A.U.	1
R_{work} (%)	14.5
R_{free} (%)	17.8
r.m.s.d. in bond lengths (Å)	0.024
r.m.s.d. in bond angles (°)	2.217
Mean B factors (Å^2)	17.35
PDB entry code	6FXW

868

869

OXIDATIVE

D-glucose 6-phosphate

↓ *G6PDH*

6-phospho D-glucono-1,5-lactone

↓ *6PGL*

D-gluconate 6-phosphate

↓ *6-PGDH*

D-ribulose 5-phosphate

NON-OXIDATIVE

RuPE ⇄   ⇄ *Rpi*

D-xylulose-5-phosphate   D-ribose 5-phosphate

⇄ *TKT* ⇄

D-glyceraldehyde 3-phosphate
D-sedoheptulose 7-phosphate

⇄ *TAL* ⇄

D-erythrose 4-phosphate   D-fructose 6-phosphate

A

Miltefosine

sKO
EC50 = 14.14
(12.61-15.86)

WT
EC50 = 16.62
(15.61-17.69)

B

338

sKO
EC50 = 19.51
(18.01 - 21.14)

WT
EC50 = 23.79
(22.75 - 24.88)

A

Thr$_{74}$
Arg$_{116}$
Asn$_{105}$
His$_{105}$
Cys$_{72}$
Arg$_{144}$
Asp$_{13}$
His$_{14}$
Arg$_{140}$

B

Thr$_{74}$
Arg$_{116}$
Asn$_{105}$
His$_{105}$
Cys$_{72}$
Arg$_{144}$
Asp$_{13}$
His$_{14}$
Arg$_{140}$

C

Thr$_{74}$
Arg$_{116}$
Asn$_{105}$
His$_{105}$
Cys$_{72}$
Arg$_{144}$
Asp$_{13}$
His$_{14}$
Arg$_{140}$

D

Thr$_{74}$
Arg$_{116}$
Asn$_{105}$
His$_{105}$
Cys$_{72}$
Arg$_{144}$
Asp$_{13}$
His$_{14}$
Arg$_{140}$